ELSEVIER

NeuroImage

www.elsevier.com/locate/ynimg
NeuroImage 34 (2007) 1650–1657

Changes in neuronal connectivity after stroke in rats as studied by serial manganese-enhanced MRI

Jet P. van der Zijden,[a,*] Ona Wu,[a,b] Annette van der Toorn,[a] Tom P. Roeling,[c] Ronald L.A.W. Bleys,[c] and Rick M. Dijkhuizen[a]

[a]*Image Sciences Institute, University Medical Center Utrecht, Bolognalaan 50, 3584 CJ, Utrecht, The Netherlands*
[b]*Athinoula A. Martinos Center for Biomedical Imaging, Massachusetts General Hospital/Massachusetts Institute of Technology/Harvard Medical School, Charlestown, MA, USA*
[c]*Rudolf Magnus Institute of Neuroscience, University Medical Center Utrecht, Utrecht, The Netherlands*

Received 21 June 2006; revised 27 October 2006; accepted 1 November 2006
Available online 18 December 2006

Loss of function and subsequent spontaneous recovery after stroke have been associated with physiological and anatomical alterations in neuronal networks in the brain. However, the spatiotemporal pattern of such changes has been incompletely characterized. Manganese-enhanced MRI (MEMRI) provides a unique tool for *in vivo* investigation of neuronal connectivity.

In this study, we measured manganese-induced changes in longitudinal relaxation rate, R_1, to assess the spatiotemporal pattern of manganese distribution after focal injection into the intact sensorimotor cortex in control rats ($n=10$), and in rats at 2 weeks after 90-min unilateral occlusion of the middle cerebral artery ($n=10$). MEMRI data were compared with results from conventional tract tracing with wheat-germ agglutinin horseradish peroxidase (WGA-HRP).

Distinct areas of the sensorimotor pathway were clearly visualized with MEMRI. At 2 weeks after stroke, manganese-induced changes in R_1 were significantly delayed and diminished in the ipsilateral caudate putamen, thalamus and substantia nigra. Loss of connectivity between areas of the sensorimotor network was also identified from reduced WGA-HRP staining in these areas on *post-mortem* brain sections. This study demonstrates that MEMRI enables *in vivo* assessment of spatiotemporal alterations in neuronal connectivity after stroke, which may lead to improved insights in mechanisms underlying functional loss and recovery after stroke.

Introduction

Stroke is the leading cause of disability in the western society. Despite acute loss of function after stroke, most patients demonstrate partial functional recovery over time. Interruption and subsequent spontaneous restoration of function have been associated with anatomical and physiological alterations of neuronal networks in the brain (Lee and van Donkelaar, 1995; Seil, 1997; Steinberg and Augustine, 1997; Weiller, 1998; Johansson, 2000). However, the spatial and temporal characteristics of neural reorganization remain largely unresolved.

In recent years, neuroimaging tools, in particular functional magnetic resonance imaging (fMRI), have been successfully applied for *in vivo*, whole-brain studies on changes in functional activation patterns in stroke patients (see reviews by Cramer and Bastings, 2000; Rijntjes and Weiller, 2002; Calautti and Baron, 2003) and animal models of stroke (Dijkhuizen et al., 2001; Dijkhuizen and Nicolay, 2003). Studies on anatomical alterations in neuronal connectivity after stroke have been mostly confined to invasive axonal tract tracing techniques (Kataoka et al., 1989; Carmichael et al., 2001; Carmichael, 2003). Manganese-enhanced MRI (MEMRI) provides a unique tool to assess changes in neuronal connections *in vivo* (Pautler et al., 1998). MEMRI is based on the detection of paramagnetic manganese (Mn^{2+}), a calcium analogue that enters active neurons through Ca^{2+} channels and is transported axonally and transsynaptically (Sloot and Gramsbergen, 1994; Pautler et al., 1998; Saleem et al., 2002). Focal injection of manganese in animal brain is followed by neuronal uptake and subsequent transport along afferent and efferent connective pathways, thereby allowing *in vivo* mapping of neuronal connections (Pautler, 2004). Allegrini and Wiessner (2003) have recently demonstrated that MEMRI has the potential to detect alterations in brain circuitry after cortical injury in rats.

The goal of our study was to depict changes in neuronal connectivity within the sensorimotor network in a rat stroke model at a time point when ischemic damage is complete and dynamic alterations in sensorimotor function have largely ceased, i.e., 2 weeks after stroke (Kawamata et al., 1997). To that aim, we characterized the spatiotemporal pattern of manganese accumula-

* Corresponding author. Fax: +31 30 2535561.
E-mail address: jet@invivonmr.uu.nl (J.P. van der Zijden).
Available online on ScienceDirect (www.sciencedirect.com).

1053-8119/$ - see front matter © 2006 Elsevier Inc. All rights reserved.
doi:10.1016/j.neuroimage.2006.11.001

tion by means of serial brain mapping of changes in the longitudinal relaxation rate R_1 ($1/T_1$), which are proportional to the local manganese concentration (Silva et al., 2004). In addition, MEMRI data were compared with a conventional neuronal tract tracing technique based on the immunohistochemical detection of the tracer wheat-germ agglutinin horseradish peroxidase (WGA-HRP) (Gong and LeDoux, 2003).

Materials and methods

Animals

All animal procedures were approved by the local ethical committee of Utrecht University and met governmental guidelines. A total of 31 male Wistar rats weighing 250–340 g were included in the study. Rats were divided into two experimental groups. Group 1 animals ($n=20$) were subjected to *in vivo* tract tracing using MEMRI; Group 2 animals ($n=11$) were subjected to conventional tract tracing using WGA-HRP immunohistochemistry. In both groups, rats were divided in two subgroups. Experimental stroke was induced in Groups 1A ($n=10$) and 2A ($n=5$). Normal rats in Groups 1B ($n=10$) and 2B ($n=6$) served as controls. Fig. 1 shows the time schedule for experimental procedures in Groups 1 and 2.

Stroke model

Rats were anesthetized with 2.5% isoflurane in N_2O/O_2 (70:30) under spontaneous respiration. Blood oxygen saturation and heart rate were continuously monitored during surgical procedures. Body temperature was maintained at 37.0±0.5°C. Transient focal cerebral ischemia was induced by a 90-min occlusion of the right middle cerebral artery (MCA) with an intraluminal filament (Longa et al., 1989). In brief, a 4.0 silicon-coated polypropylene suture (Ethicon, Piscataway, NJ, USA) was introduced into the external carotid artery and advanced through the internal carotid artery until a slight resistance was felt, indicating that the MCA was occluded. After 90 min, the filament was withdrawn from the internal carotid artery to allow reperfusion. After surgery, rats received a subcutaneous injection of 0.3 mg/kg buprenorphin (Schering-Plough, Utrecht, The Netherlands) for post-surgical pain relief, and 5 ml saline to compensate for loss of water and minerals.

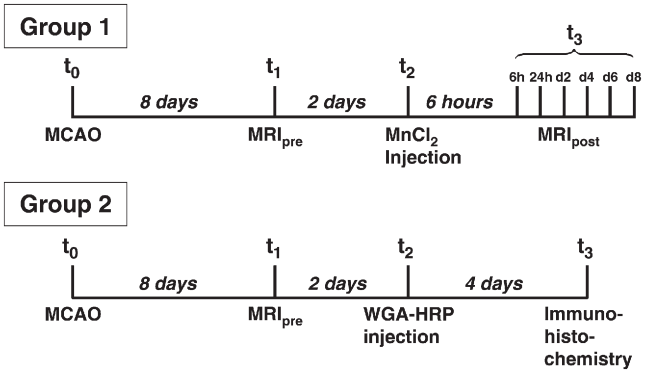

Fig. 1. Schematic representation of the time schedule of experimental procedures for Groups 1 and 2. t_0: MCA occlusion (MCAO); t_1: MRI of ischemic lesion (MRI_{pre}); t_2: injection of tracer ($MnCl_2$ or WGA-HRP); t_3: tracer detection with MRI or immunohistochemistry.

Tracer injection

Neuronal tract tracer was injected at 10 days after MCA occlusion. Animals were anesthetized by subcutaneous injection of a mixture of 0.55 mg/kg midazolam and 0.315 mg/ml fentanyl citrate and 10 mg/ml fluanisone (0.55 mg/kg). Rats were placed in a stereotactic holder and immobilized by earplugs and a tooth-holder. Blood oxygen saturation and heart rate were continuously monitored. Body temperature was maintained at 37.0±0.5°C.

A burr hole was drilled in the skull at 0.5 mm anterior and 1.5–3.0 mm lateral to bregma (according to Paxinos and Watson, 1998). Lateral coordinates were adapted based on the extent of the lesion, as determined by T_2-weighted MRI prior to tracer injection (see below), and chosen as such that tracer was injected in spared sensorimotor cortical tissue bordering the T_2-defined infarct. Injections sites for control animals were adjusted correspondingly. Mean lateral coordinates were the same for control rats (2.5±0.7 mm) and for rats with a stroke (2.5±0.7 mm).

0.2 µl 1 M isotonic $MnCl_2$ (Group 1) or 0.2 µl 5% WGA-HRP (Group 2) was injected at 1.5 mm below the dura, with a 2.0 µl Hamilton syringe at a rate of 0.05 µl/min. After injection, the needle was left in place for 3 min to prevent leakage.

MRI

MRI measurements were performed on a 4.7 T horizontal bore MR system (Varian, Palo Alto, CA, USA) with the use of a Helmholtz volume coil (90-mm diameter) and an inductively coupled surface coil (35-mm diameter) for signal excitation and detection, respectively.

Prior to MRI, rats were anesthetized with 4% isoflurane for endotracheal intubation followed by mechanical ventilation with 2.5% isoflurane in N_2O/O_2 (70:30). Rats were placed in an MR-compatible stereotactic holder and immobilized with earplugs and a toothholder. Blood oxygen saturation and heart rate were monitored during MRI measurements, and body temperature was maintained at 37.0±0.5°C.

First, T_2-weighted MRI (multi-echo acquisition with repetition time (TR)=3 s; echo time (TE)=17.5 ms; echo train length=8; acquisition matrix=128×128; voxel dimensions=0.25×0.25×1.2-mm^3; 15 coronal slices; number of averages=2; total acquisition time=12 min and 48 s) was performed in all rats with a stroke at 2 days prior to tracer injection to determine the extent of the ischemic lesion. In addition, in rats of Group 1, pre-contrast T_1-weighted MRI was performed using a saturation recovery gradient-echo sequence with seven TRs (TR/TE=55–3000/18 ms; acquisition matrix=128×128; voxel dimensions=0.25×0.25×1.2 mm^3; 15 coronal slices; number of averages=2; total acquisition time=26 min and 16 s). Subsequently, T_2- and T_1-weighted MRI were performed at day 2, 4, 6 and 8 after manganese injection. In a number of animals (Group 1A, $n=5$; Group 1B, $n=5$), MRI was also done at 6 and 24 h after manganese injection.

Immunohistochemistry

At 4 days after WGA-HRP injection, Group 2 rats were deeply anesthetized by intraperitoneal injection of pentobarbital (120 mg/kg) and immediately transcardially perfused with saline

followed by 4% paraformaldehyde in 0.1 M phosphate-buffered saline (PBS). Brains were removed and post-fixed in 4% paraformaldehyde in 0.1 M PBS for an additional 2 h and subsequently stored in 20% sucrose in 0.1 M PBS at 4°C. Brains were cut in 40-μm-thick coronal sections on a freezing microtome and stored in 20% sucrose in 0.1 M PBS. Free-floating sections were processed for immunohistochemical detection of WGA-HRP using the following protocol: (1) 3×10-min rinsing in Tris-buffered saline (TBS) (0.05 M; pH 7.6); (2) 60-min rinsing in 3% H_2O_2 in TBS; (3) 3×10-min rinsing in TBS; (4) 60-min pre-incubation with 3% normal rabbit serum in TBS; (5) overnight incubation with primary antibody (goat anti-WGA (Vector Laboratories, Burlingame, CA, USA); 1:500), 0.1% bovine serum albumin and 0.1% Triton X-100 in TBS at 4°C; (6) 3×10-min rinsing in TBS; (7) 60-min incubation with secondary antibody (polyclonal rabbit anti-goat IgG (DakoCytomation, Glostrup, Denmark); 1:250), 0.1% bovine serum albumin and 0.1% Triton X-100 in TBS; (8) 3×10-min rinsing in TBS; (9) 90-min incubation with peroxidase–antiperoxidase complex (1:600), 0.1% Triton X-100 in TBS; (10) 3×10-min rinsing in TBS; (11) development using a diaminobenzidine peroxidase substrate kit (Vector Laboratories Burlingame, CA, USA) with nickel intensification according to manufacturer's instructions; (12) 3×10-min rinsing in TBS; (13) overnight air drying, dehydration and coverslipping with Entallan (Merck, Darmstadt, Germany).

Data analysis

MRI

Quantitative T_2 maps were calculated on a voxel-wise basis by weighted linear least-squares fit of the logarithm of the signal intensity at different echo times.

Lesion volumes were determined from 11 adjacent slices on quantitative T_2 maps as ipsilateral tissue greater than the mean +2 SD of T_2 in contralateral tissue. The edema-corrected hemispheric lesion volume (%HLV^e) was calculated as described by Gerriets et al. (2004):

$$\%HLV^e = (HV_c - (HV_i - LV^u))/HV^c \times 100\%, \quad (1)$$

where HV_c and HV_i are the contralateral and ipsilateral hemispheric volumes, respectively; and LV^u is the uncorrected lesion volume.

Quantitative T_1 maps were calculated on a voxel-wise basis by performing a non-linear least-squares fit using the Levenberg–Marquardt method (Press and Vetterling, 1992). Longitudinal relaxation rate R_1 ($1/T_1$) maps were coregistered to an averaged brain T_2-weighted MRI data set from 6 control rats using semi-automated image registration software (MNI Autoreg (Collins et al., 1994)). To correct for misregistration as a result of edema-induced brain distortion, anatomic landmarks were manually selected on brains with a stroke lesion followed by a second registration procedure. Changes in R_1 after manganese administration are proportional to the local manganese concentration (Silva et al., 2004). Hence, manganese accumulation was measured in specific regions-of-interest (ROIs) from the difference between pre- and post-contrast R_1 (ΔR_1). We selected four ipsi- and contralateral ROIs within the sensorimotor corticostriatonigral-thalamocortical pathway. Based on the extent of the lesion in animals with a stroke, ROI size and shape were adjusted, so that the ROI included that part of the particular brain region that was invariably outside the lesion area for all animals. Contralateral ROIs were exactly matched in size and shape with respect to their ipsilateral counterparts. There were no significant differences between T_2 values in the ipsi- and contralateral ROIs (paired Student's t-test; $P<0.05$), which confirms that ROIs were not part of the infarcted area. Thus, for all animals, ROIs were the same in location, size and shape, and only included the non-infarcted part of the specific anatomical structure.

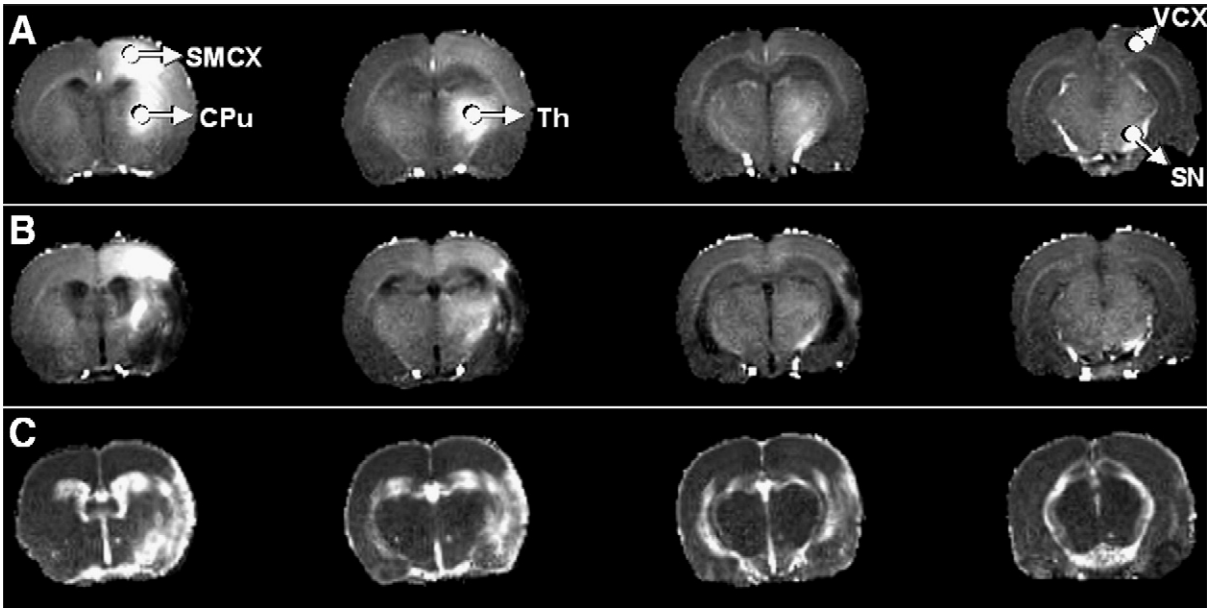

Fig. 2. R_1 maps of four adjacent coronal brain slices at 2 days after $MnCl_2$ injection in the ipsilateral sensorimotor cortex of a control rat (A) and 2 weeks after unilateral stroke (B). (C) T_2 maps of the same animal as in (B) at 2 days before manganese injection (i.e., 8 days after stroke). Manganese-induced contrast enhancement is clear in the ipsilateral sensorimotor cortex (SMCX), caudate putamen (CPu), thalamus (Th) and substantia nigra (SN) and minor in the ipsilateral visual cortex (VCX). After stroke, manganese enhancement was less in subcortical areas. The lesion is characterized by reduced R_1 and prolonged T_2.

The selected ROIs were the sensorimotor cortex (SMCX; 36 voxels; center at 1.0 mm posterior, 1.5 mm lateral and 1.5 mm depth from bregma (Paxinos and Watson, 1998)), caudate putamen (CPu; 34 voxels; center at 1.0 mm posterior, 3.0 mm lateral and 5.5 mm depth from bregma), thalamus (Th; 87 voxels; center at 2.5 mm posterior, 2.5 mm lateral and 6.0 mm depth from bregma) and substantia nigra (SN; 15 voxels; center at 5.5 mm posterior, 1.5 mm lateral and at a depth of 8.5 mm from bregma) (see Fig. 2A). An ROI was also placed in the visual cortex (VCX; 45 voxels; center at 5.5 mm posterior, 3.0 mm lateral and 1.5 mm depth from bregma) to check for non-specific distribution of manganese.

Immunohistochemistry

WGA-HRP-stained brain slices were studied with a light microscope (Zeiss Axiophot with Sony 3 CCD Color Video Camera) under bright- and dark-field illumination. WGA-HRP-labeled cells were counted with Kontron KS 400 software in anatomical areas that matched the ROIs used for MRI analysis (5 adjacent sections were analyzed for each ROI).

Statistics

All values are expressed as mean±SD. Differences in the temporal pattern of manganese enhancement were analyzed using a one- (within ROIs) or two-way (between ROIs, and between groups) repeated measures analysis of variance (ANOVA) with post-hoc multiple comparison *t*-testing with Bonferroni correction. Differences in lesion volumes, T_2 values and WGA-HRP staining were statistically analyzed with a paired or unpaired Student's *t*-test. $P<0.05$ was considered significant.

Results

Ischemic damage

In rats with a stroke, the unilateral ischemic lesion was characterized by a prolonged T_2 (see Fig. 2C). The mean % HLV^e was 12.3±4.8%, with no significant difference in lesion volumes between Group 1 and 2 (13.1±3.2% and 11.0±6.9%, respectively).

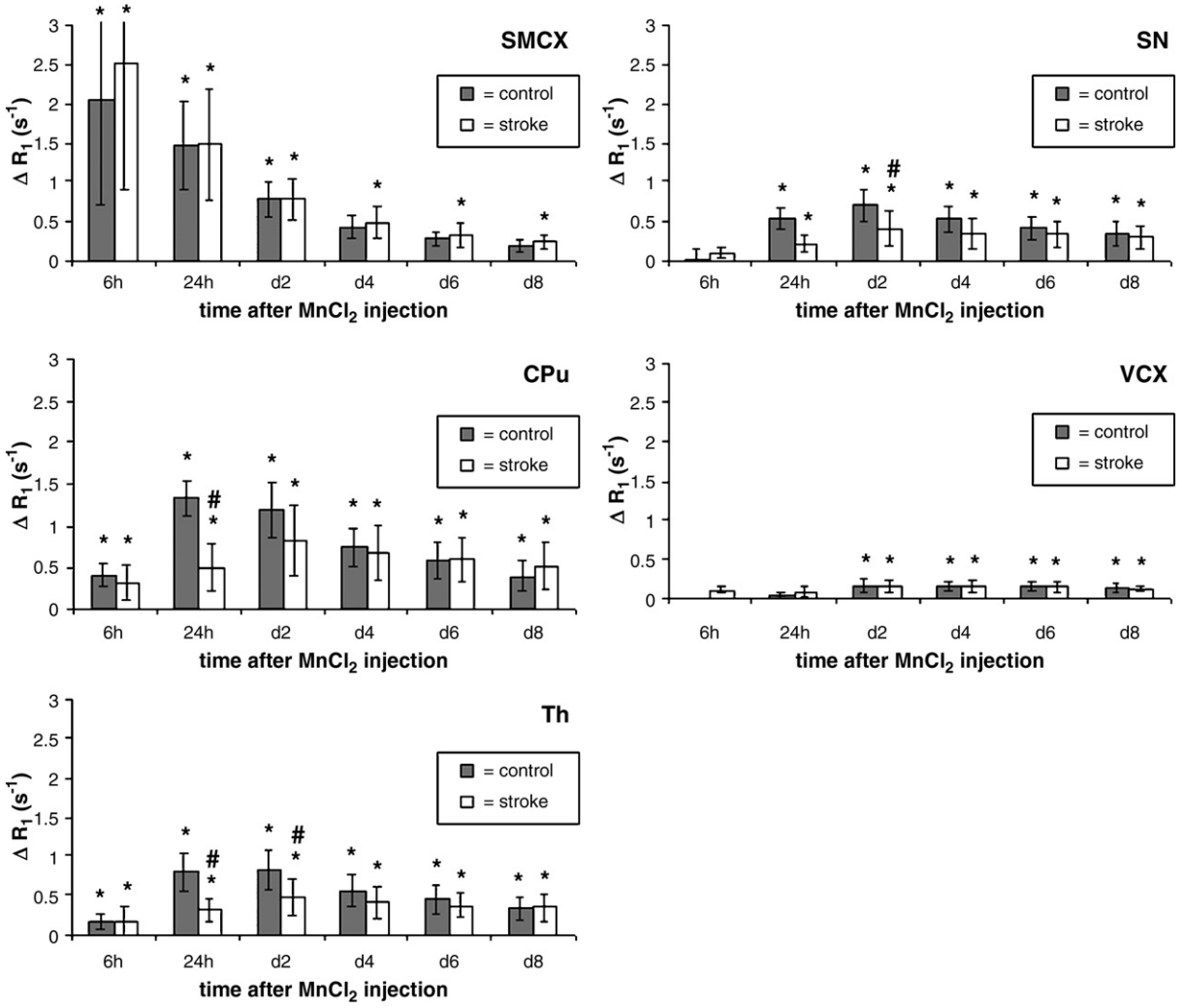

Fig. 3. Manganese-induced ΔR_1 (s^{-1})±SD in ipsilateral ROIs as a function of time (6 h and 24 h ($n=5$), and 2, 4, 6 and 8 days ($n=10$)) after $MnCl_2$ injection in the ipsilateral sensorimotor cortex in control rats (■) and after stroke (□). SMCX: sensorimotor cortex; CPu: caudate putamen; Th: thalamus; SN: substantia nigra; VCX: visual cortex. *$P<0.05$, post-manganese R_1 larger than pre-manganese R_1. #$P<0.05$, stroke vs. control group. Among all time points, there was an overall significant difference in ΔR_1 in Th between control rats and rats with a stroke ($P<0.05$).

Injection site

Lateral coordinates of tracer injection site varied between 1.5 and 3.0 mm from bregma (see Materials and methods section), but were invariably in the forelimb area of the sensorimotor cortex. To determine if variations in injection site influence the pattern of tracer distribution, control animals in Groups 1B and 2B were divided into 2 subgroups, based on the lateral coordinates of the injection site. In subgroup I, lateral coordinates were 1.5–2.5 mm from bregma ($n=4$ in Group 1B; $n=3$ in Group 2B). In subgroup II, lateral coordinates were 3.0 mm from bregma ($n=6$ in Group 1B; $n=3$ in Group 2B). There was only a significant difference in manganese-induced ΔR_1 in SMCX, i.e., nearby the injection site, between the two subgroups. In all other ROIs, there were no significant differences in ΔR_1 values between the subgroups. Moreover, there were no significant differences between the subgroups in any of the ROIs with regard to number of WGA-HRP-labeled cells. Therefore, we conclude that the small variation in site of injection did not result in different global patterns of manganese enhancement or WGA-HRP staining.

MEMRI

The spatial pattern of manganese enhancement was clearly visualized on R_1 maps (Figs. 2A and B). R_1 increase was observed in all four ROIs of the ipsilateral sensorimotor network in control rats as well as after stroke. The temporal pattern of manganese-induced R_1 changes in ipsilateral ROIs is shown in Fig. 3. R_1 values were significantly increased from baseline R_1 as early as 6 h after manganese injection in SMCX, CPu and Th. In SN, manganese-induced R_1 change became significant after 24 h. After a peak, ΔR_1 subsequently declined. In SMCX in control rats, post-manganese R_1 values were not significantly elevated after ≥4 days. For each ROI, we defined the time point of maximal ΔR_1 as the time point at which ΔR_1 was significantly higher than ΔR_1 values at the largest number of other time points. Close to the injection site in SMCX, ΔR_1 was maximal at 6 h after manganese administration in control and stroke rats. In CPu, ΔR_1 was maximal after 24 h/2 days in control rats and after 2 days in stroke rats. In Th and SN, ΔR_1 was maximal after 2 days in control and stroke rats. ΔR_1 values in the ROIs at later time points were significantly reduced as compared to the maximal ΔR_1: in SMCX after ≥24 h in control and stroke rats; in

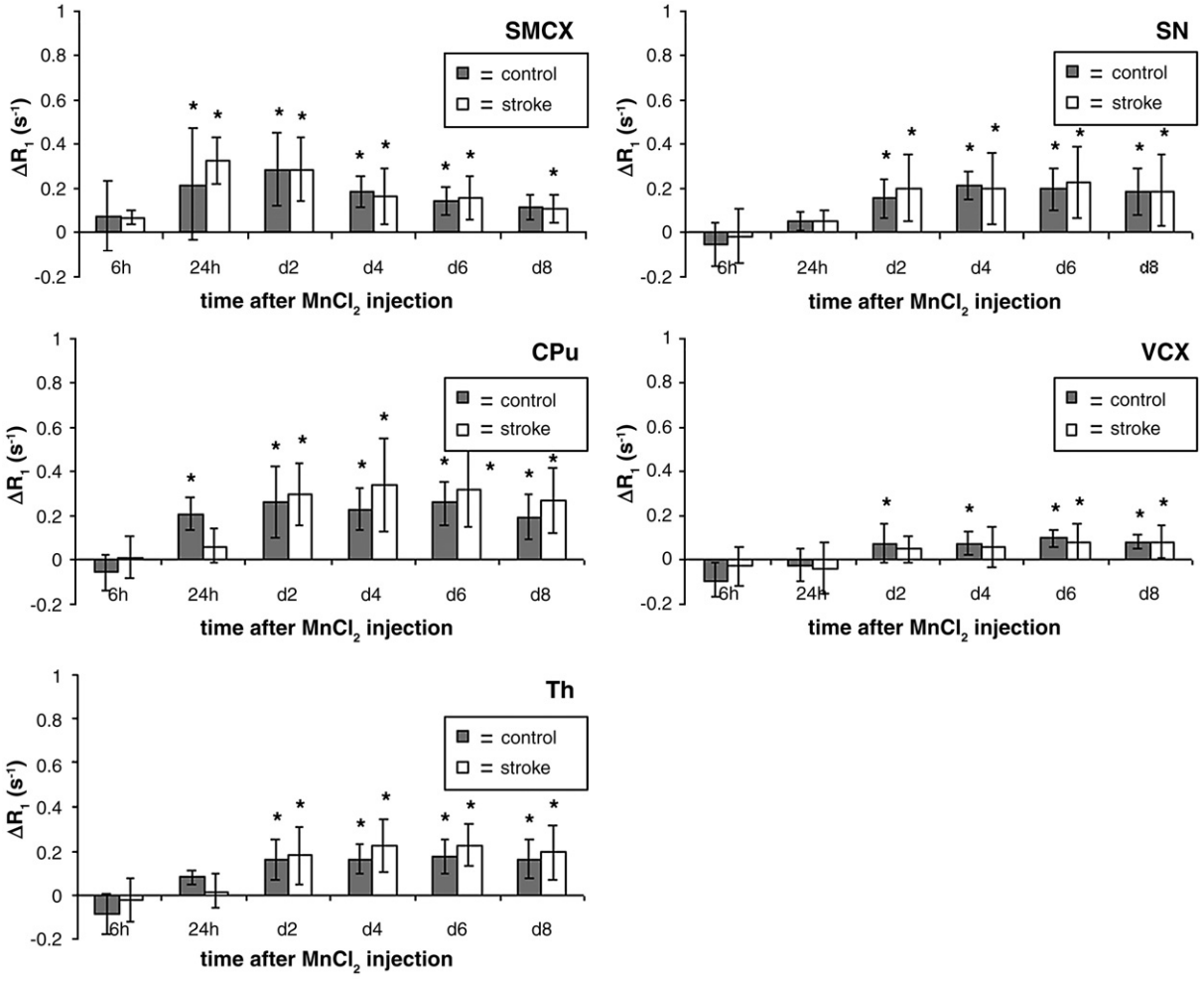

Fig. 4. Manganese-induced ΔR_1 (s^{-1})±SD in contralateral ROIs as a function of time (6 h and 24 h ($n=5$), and 2, 4, 6 and 8 days ($n=10$)) after $MnCl_2$ injection in the ipsilateral sensorimotor cortex in control rats (■) and after stroke (□). SMCX: sensorimotor cortex; CPu: caudate putamen; Th: thalamus; SN: substantia nigra; VCX: visual cortex. *$P<0.05$, post-manganese R_1 larger than pre-manganese R_1.

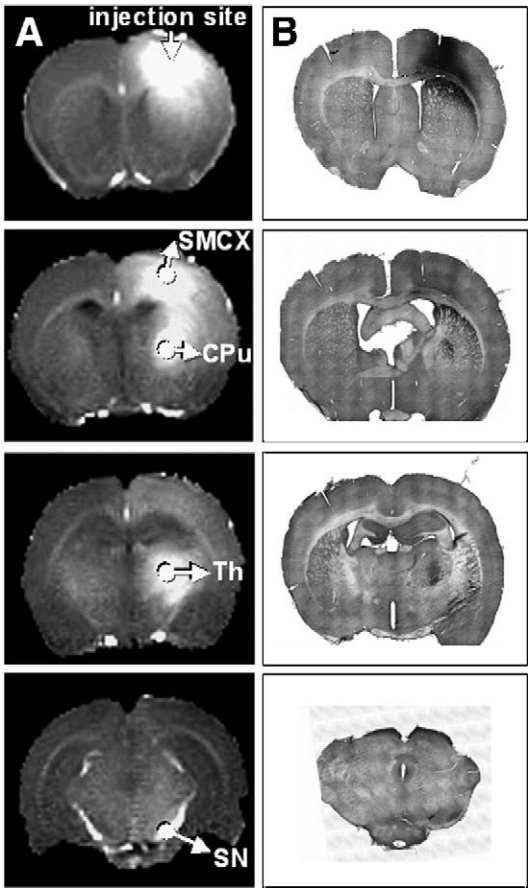

Fig. 5. R_1 maps (A) and corresponding histological sections (B) of five adjacent slices of control rat brains at 2 days after $MnCl_2$ injection and at 4 days after WGA-HRP injection, respectively, into the ipsilateral sensorimotor cortex. Manganese-induced R_1 increase and WGA-HRP cell labeling are evident at the injection site and in the sensorimotor cortex (SMCX), caudate putamen (CPu), thalamus (Th) and substantia nigra (SN). Note that upper cerebral tissue was detached during preparation of the most posterior histological section.

CPu after ≥4 days in control rats, and after ≥6 days in stroke rats; in Th after ≥4 days in control rats, and after ≥8 days in stroke rats; and in SN after ≥4 days in control rats. In SN in stroke rats, ΔR_1 did not significantly decrease within the 8 days of MEMRI measurements.

Small but significant manganese-induced R_1 increases were also detected in VCX (Fig. 3) and in contralateral sensorimotor ROIs (Fig. 4). ΔR_1 changes in ipsi- and contralateral VCX, however, were significantly lower than ΔR_1 changes in sensorimotor ROIs within the same hemisphere. For example, in control rats maximal ΔR_1 in ipsi- and contralateral VCX were $0.16 \pm 0.06\ s^{-1}$ and $0.10 \pm 0.04\ s^{-1}$, as compared to $1.34 \pm 0.21\ s^{-1}$ and $0.26 \pm 0.16\ s^{-1}$ in ipsi- and contralateral CPu, respectively.

After stroke, manganese-induced ΔR_1 changes were significantly reduced in the CPu at 24 h, in the Th at 24 h and 2 days, and in the SN at 2 days after manganese injection (Fig. 3). A significant main group effect (stroke vs. control rats) was found for ΔR_1 in Th ($P<0.05$). We found no significant correlation between lesion volume and decrease in ΔR_1 at any time point in any of the ROIs. Also, we found no statistically significant differences in contralateral ROIs between control rats and rats with a stroke, however, there was a trend for larger ΔR_1 values in contralateral CPu and Th after stroke, as compared to control animals ($P=0.10$ and $P=0.07$, respectively).

Immunohistochemistry

The spatial pattern of WGA-HRP staining corresponded well with that of manganese enhancement. WGA-HRP-labeled cells were found in all ROIs in the ipsilateral sensorimotor network, both in control rats and after stroke (Fig. 5). There were, however, differences in the degree of tracer accumulation when comparing WGA-HRP staining with MEMRI data. For example, the spatial extent of manganese enhancement was larger than that of WGA-HRP labeling. Furthermore, at variance with MEMRI data, in control rats WGA-HRP labeling was strongest in the thalamus (147 ± 59 cells) as compared to other ROIs (SMCX: 81 ± 29 cells;

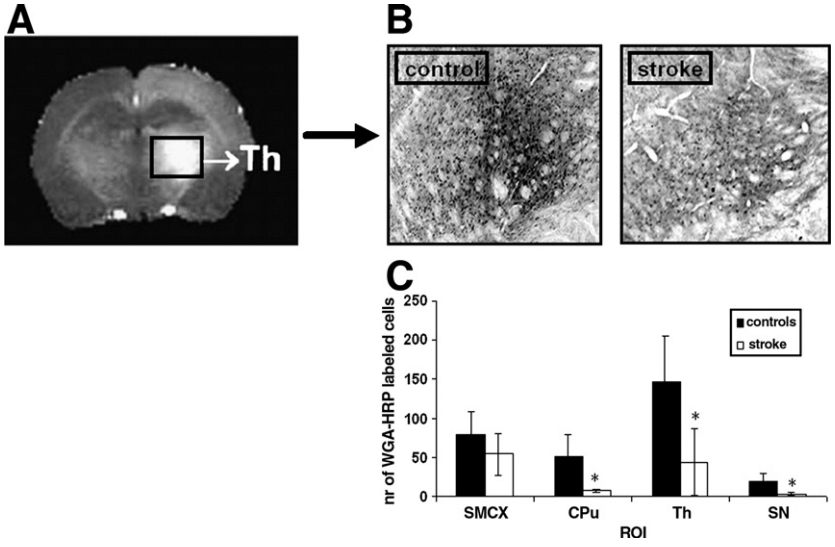

Fig. 6. R_1 map (A) and corresponding histological sections of a control and a stroke rat brain (magnification 16×) (B) showing increased R_1 and cell labeling in the ipsilateral thalamus (Th) at 2 days after injection of $MnCl_2$ and 4 days after injection of WGA-HRP into the ipsilateral sensorimotor cortex (SMCX). After stroke, the number of WGA-HRP-labeled cells was significantly reduced in the ipsilateral caudate putamen (CPu), Th and substantia nigra (SN) (B, C). *$P<0.05$, stroke vs. control group.

CPu: 51±30 cells; SN: 20±10 cells) ($P<0.05$). Also, we found no WGA-HRP-labeled cells in ipsilateral VCX and in contralateral ROIs. After stroke, WGA-HRP staining was significantly reduced in the ipsilateral CPu ($P=0.01$), Th ($P=0.01$) and SN ($P=0.004$) as compared to control rats (Fig. 6).

Discussion

In this study, we characterized the spatiotemporal distribution of the paramagnetic neuronal tract tracer manganese using *in vivo* MRI in order to assess changes in neuronal connectivity within the sensorimotor network at 2 weeks after unilateral stroke in rats. In addition, MEMRI data were compared with results from a conventional tract tracing method based on *post-mortem* detection of WGA-HRP labeling in the brain.

Manganese-induced R_1 changes were detected in distinct regions of the connective pathway between cortex, caudate putamen, substantia nigra and thalamus after injection of manganese in the sensorimotor cortex. Manganese is taken up by neurons through calcium channels and may be transported anterogradely and retrogradely along the axons (Pautler et al., 2003). The manganese-induced R_1 increase we observed in the substantia nigra, which mostly receives indirect projections from the sensorimotor cortex, confirms the findings by Pautler et al. (1998) and Saleem et al. (2002) that manganese can be transferred transsynaptically. In control rats, maximal cortical contrast enhancement occurred within 6 h after manganese administration followed by maximal R_1 increase in the caudate putamen around 24 h, and in the thalamus and substantia nigra at 2 days. R_1 changes diminished thereafter, but were still evident at 8 days after manganese injection. In rats with a two-week-old unilateral stroke, manganese-induced ΔR_1 was significantly diminished at the time points of maximal manganese enhancement in subcortical areas, i.e., the caudate putamen, substantia nigra and, in particular, the thalamus. The reduced build-up of manganese in these regions points toward disturbed connectivity within the sensorimotor network, even though manganese was injected in preserved cortical tissue.

WGA-HRP labeling was found in the same regions of the ipsilateral sensorimotor pathway as detected with MEMRI, which is in agreement with a previous study in monkeys by Saleem et al. (2002). The spatial extent of manganese enhancement, however, was larger than that of WGA-HRP labeling. This may be explained by a relatively higher concentration and/or more diffusion of manganese at the injection site. In addition, partial volume effects on MRI slices that were about thirty-fold thicker than histological sections may have caused more blurring. WGA-HRP labeling was strongest in the thalamus, which is probably due to the relatively high number of thalamocortical afferents. Although WGA-HRP is transported antero- and retrogradely, our results indicate that transport was predominantly in retrograde direction (see also Kobbert et al., 2000; Oztas, 2003). In correspondence with our MEMRI data, after stroke, a reduction of WGA-HRP-labeled cells was found in subcortical areas.

Our results correspond with earlier reports on post-stroke loss of efferent thalamocortical pathways based on *ex vivo* detection of neuronal tract tracer (Kataoka et al., 1989; Iizuka et al., 1990; Carmichael et al., 2001). Cerebral ischemia has been shown to affect remote areas that are connected to the lesion site through anterograde and/or retrograde axonal degeneration (Iizuka et al., 1989; Kataoka et al., 1989). In addition to axonal disconnection, breakdown of axonal cytoskeletal components and disruption of axoplasmic transport, which have been described after MCA occlusion in rats (Yam et al., 1998), may account for the observed loss of tracer accumulation within the sensorimotor network.

Importantly, serial *in vivo* MEMRI may provide exclusive information on axonal transport dynamics. For example, in ipsilateral CPu of rats with a stroke maximal manganese-induced ΔR_1 occurred later than in control rats. Moreover, in all subcortical ROIs, subsequent ΔR_1 decrease was significantly delayed. These results point toward delayed neuronal tracer arrival and clearance after stroke.

Slight, but significant manganese enhancement was detected in areas outside the sensorimotor network, e.g., the visual cortex. This may be explained by passive diffusion and/or systemic reabsorption into the microvessels and cerebral spinal fluid (see also Watanabe et al., 2004; Thuen et al., 2005). Non-specific passive manganese distribution, however, was minor as compared to the network-specific axonal transport to sensorimotor areas. Small, but significant manganese enhancement was also observed in contralateral sensorimotor cortex, caudate putamen, thalamus and substantia nigra. Manganese-induced R_1 changes in these contralateral sensorimotor regions were significantly higher than R_1 changes in ipsi- and contralateral visual cortex. Maximal manganese-induced ΔR_1 in contralateral caudate putamen was about a factor 1.5–2 higher than ΔR_1 in the ipsilateral visual cortex, while these ROIs are at comparable distance from the manganese injection site (5.7 mm and 6.0 mm respectively (Paxinos and Watson, 1998)). These findings suggest that manganese enhancement in the contralateral sensorimotor network cannot be merely explained by non-specific manganese accumulation, and anyway involves transhemispheric axonal transport.

We detected slightly elevated contralateral manganese enhancement in rats with a stroke as compared to controls, however, differences were not statistically significant. Increased transhemispheric connectivity after stroke has been previously described, but was observed at stages much later than 2 weeks post-stroke (Carmichael, 2003; Allegrini and Wiessner, 2003). To assess potential plasticity-associated changes in connectivity between the injured and unaffected hemisphere after stroke with MEMRI, future studies should include more chronic time points after stroke.

Conclusion

Our study demonstrates that MEMRI allows unique spatiotemporal assessment of alterations in neuronal connectivity after stroke. We have detected decreased and delayed manganese enhancement in brain network regions that are connected to the sensorimotor cortex where manganese was injected. Loss or dysfunction of neuronal connections, even outside the ischemic lesion, may explain the lasting impairment of function. MEMRI thereby provides a unique *in vivo* tool that can give important new insights in neural correlates of functional loss and recovery after stroke.

Acknowledgments

Dr. Dijkhuizen is financially supported by a fellowship of the Royal Netherlands Academy of Arts and Sciences.

We thank Gerard van Vliet and Jan-Willem de Groot for excellent technical assistance.

References

Allegrini, P.R., Wiessner, C., 2003. Three-dimensional MRI of cerebral projections in rat brain in vivo after intracortical injection of MnCl2. NMR Biomed. 16, 252–256.

Calautti, C., Baron, J.C., 2003. Functional neuroimaging studies of motor recovery after stroke in adults: a review. Stroke 34, 1553–1566.

Carmichael, S.T., 2003. Plasticity of cortical projections after stroke. Neuroscientist 9, 64–75.

Carmichael, S.T., Wei, L., Rovainen, C.M., Woolsey, T.A., 2001. New patterns of intracortical projections after focal cortical stroke. Neurobiol. Dis. 8, 910–922.

Collins, D.L., Neelin, P., Peters, T.M., Evans, A.C., 1994. Automatic 3D intersubject registration of MR volumetric data in standardized Talairach space. J. Comput. Assist. Tomogr. 18, 192–205.

Cramer, S.C., Bastings, E.P., 2000. Mapping clinically relevant plasticity after stroke. Neuropharmacology 39, 842–851.

Dijkhuizen, R.M., Nicolay, K., 2003. Magnetic resonance imaging in experimental models of brain disorders. J. Cereb. Blood Flow Metab. 23, 1383–1402.

Dijkhuizen, R.M., Ren, J., Mandeville, J.B., Wu, O., Ozdag, F.M., Moskowitz, M.A., Rosen, B.R., Finklestein, S.P., 2001. Functional magnetic resonance imaging of reorganization in rat brain after stroke. Proc. Natl. Acad. Sci. U. S. A. 98, 12766–12771.

Gerriets, T., Stolz, E., Walberer, M., Muller, C., Rottger, C., Kluge, A., Kaps, M., Fisher, M., Bachmann, G., 2004. Complications and pitfalls in rat stroke models for middle cerebral artery occlusion: a comparison between the suture and the macrosphere model using magnetic resonance angiography. Stroke 35, 2372–2377.

Gong, S., LeDoux, M.S., 2003. Immunohistochemical detection of wheat germ agglutinin-horseradish peroxidase (WGA-HRP). J. Neurosci. Methods 126, 25–34.

Iizuka, H., Sakatani, K., Young, W., 1989. Corticofugal axonal degeneration in rats after middle cerebral artery occlusion. Stroke 20, 1396–1402.

Iizuka, H., Sakatani, K., Young, W., 1990. Neural damage in the rat thalamus after cortical infarcts. Stroke 21, 790–794.

Johansson, B.B., 2000. Brain plasticity and stroke rehabilitation. The Willis lecture. Stroke 31, 223–230.

Kataoka, K., Hayakawa, T., Yamada, K., Mushiroi, T., Kuroda, R., Mogami, H., 1989. Neuronal network disturbance after focal ischemia in rats. Stroke 20, 1226–1235.

Kawamata, T., Dietrich, W.D., Schallert, T., Gotts, J.E., Cocke, R.R., Benowitz, L.I., Finklestein, S.P., 1997. Intracisternal basic fibroblast growth factor enhances functional recovery and up-regulates the expression of a molecular marker of neuronal sprouting following focal cerebral infarction. Proc. Natl. Acad. Sci. U. S. A. 94, 8179–8184.

Kobbert, C., Apps, R., Bechmann, I., Lanciego, J.L., Mey, J., Thanos, S., 2000. Current concepts in neuroanatomical tracing. Prog. Neurobiol. 62, 327–351.

Lee, R.G., van Donkelaar, P., 1995. Mechanisms underlying functional recovery following stroke. Can. J. Neurol. Sci. 22, 257–263.

Longa, E.Z., Weinstein, P.R., Carlson, S., Cummins, R., 1989. Reversible middle cerebral artery occlusion without craniectomy in rats. Stroke 20, 84–91.

Oztas, E., 2003. Neuronal tracing. Neuroanatomy 2, 2–5.

Pautler, R.G., 2004. In vivo, trans-synaptic tract-tracing utilizing manganese-enhanced magnetic resonance imaging (MEMRI). NMR Biomed. 17, 595–601.

Pautler, R.G., Silva, A.C., Koretsky, A.P., 1998. In vivo neuronal tract tracing using manganese-enhanced magnetic resonance imaging. Magn. Reson. Med. 40, 740–748.

Pautler, R.G., Mongeau, R., Jacobs, R.E., 2003. In vivo trans-synaptic tract tracing from the murine striatum and amygdala utilizing manganese enhanced MRI (MEMRI). Magn. Reson. Med. 50, 33–39.

Paxinos, G., Watson, C., 1998. The Rat Brain in Stereotaxic Coordinates. Academic Press, San Diego.

Press, W.H., Vetterling, W.T., 1992. Numerical Recipes in FORTRAN: The Art of Scientific Computing. Cambridge University Press, Cambridge, England.

Rijntjes, M., Weiller, C., 2002. Recovery of motor and language abilities after stroke: the contribution of functional imaging. Prog. Neurobiol. 66, 109–122.

Saleem, K.S., Pauls, J.M., Augath, M., Trinath, T., Prause, B.A., Hashikawa, T., Logothetis, N.K., 2002. Magnetic resonance imaging of neuronal connections in the macaque monkey. Neuron 34, 685–700.

Seil, F.J., 1997. Recovery and repair issues after stroke from the scientific perspective. Curr. Opin. Neurol. 10, 49–51.

Silva, A.C., Lee, J.H., Aoki, I., Koretsky, A.P., 2004. Manganese-enhanced magnetic resonance imaging (MEMRI): methodological and practical considerations. NMR Biomed. 17, 532–543.

Sloot, W.N., Gramsbergen, J.B., 1994. Axonal transport of manganese and its relevance to selective neurotoxicity in the rat basal ganglia. Brain Res. 657, 124–132.

Steinberg, B.A., Augustine, J.R., 1997. Behavioral, anatomical, and physiological aspects of recovery of motor function following stroke. Brain Res. Brain Res. Rev. 25, 125–132.

Thuen, M., Singstad, T.E., Pedersen, T.B., Haraldseth, O., Berry, M., Sandvig, A., Brekken, C., 2005. Manganese-enhanced MRI of the optic visual pathway and optic nerve injury in adult rats. J. Magn. Reson. Imaging 22, 492–500.

Watanabe, T., Frahm, J., Michaelis, T., 2004. Functional mapping of neural pathways in rodent brain in vivo using manganese-enhanced three-dimensional magnetic resonance imaging. NMR Biomed. 17, 554–568.

Weiller, C., 1998. Imaging recovery from stroke. Exp. Brain Res. 123, 13–17.

Yam, P.S., Dewar, D., McCulloch, J., 1998. Axonal injury caused by focal cerebral ischemia in the rat. J. Neurotrauma 15, 441–450.